ORIGINAL ARTICLE

JBMR

Regulator of G Protein Signaling Protein 12 (Rgs12) Controls Mouse Osteoblast Differentiation via Calcium Channel/Oscillation and Gαi-ERK Signaling

Ziqing Li,[1*] Tongjun Liu,[2,3,4*] Alyssa Gilmore,[2*] Néstor Más Gómez,[1] Chuanyun Fu,[1,5] Jormay Lim,[1] Shuting Yang,[1] Claire H Mitchell,[1,6] Yi-ping Li,[7] Merry J Oursler,[8] and Shuying Yang[1,2,9]

[1]Department of Anatomy and Cell Biology, School of Dental Medicine, University of Pennsylvania, Philadelphia, PA, USA
[2]Department of Oral Biology, School of Dental Medicine, University of Buffalo, State University of New York, Buffalo, NY, USA
[3]Department of Implantology, Shandong Provincial Key Laboratory of Oral Biomedicine, School of Stomatology, Jinan, Shandong, China
[4]Department of Stomatology, Jinan Central Hospital Affiliated to Shandong University, Jinan, Shandong, China
[5]Department of Stomatology, Shandong Provincial Hospital Affiliated to Shandong University, Jinan, Shandong, China
[6]Department of Physiology, School of Medicine, University of Pennsylvania, Philadelphia, PA, USA
[7]Department of Pathology, University of Alabama at Birmingham, Birmingham, AL, USA
[8]Department of Medicine, Endocrine Research Unit, Mayo Clinic, Rochester, MN, USA
[9]The Penn Center for Musculoskeletal Disorders, School of Medicine, University of Pennsylvania, Philadelphia, PA, USA

ABSTRACT

Bone homeostasis intimately relies on the balance between osteoblasts (OBs) and osteoclasts (OCs). Our previous studies have revealed that regulator of G protein signaling protein 12 (Rgs12), the largest protein in the Rgs super family, is essential for osteoclastogenesis from hematopoietic cells and OC precursors. However, how Rgs12 regulates OB differentiation and function is still unknown. To understand that, we generated an OB-targeted Rgs12 conditional knockout (CKO) mice model by crossing $Rgs12^{fl/fl}$ mice with Osterix (Osx)-Cre transgenic mice. We found that Rgs12 was highly expressed in both OB precursor cells (OPCs) and OBs of wild-type (WT) mice, and gradually increased during OB differentiation, whereas Rgs12-CKO mice ($Osx^{Cre/+}$; $Rgs12^{fl/fl}$) exhibited a dramatic decrease in both trabecular and cortical bone mass, with reduced numbers of OBs and increased apoptotic cell population. Loss of Rgs12 in OPCs in vitro significantly inhibited OB differentiation and the expression of OB marker genes, resulting in suppression of OB maturation and mineralization. Further mechanism study showed that deletion of Rgs12 in OPCs significantly inhibited guanosine triphosphatase (GTPase) activity and cyclic adenosine monophosphate (cAMP) level, and impaired Calcium (Ca^{2+}) oscillations via restraints of major Ca^{2+} entry sources (extracellular Ca^{2+} influx and intracellular Ca^{2+} release from endoplasmic reticulum), partially contributed by the blockage of L-type Ca^{2+} channel mediated Ca^{2+} influx. Downstream mediator extracellular signal-related protein kinase (ERK) was found inactive in OBs of $Osx^{Cre/+}$; $Rgs12^{fl/fl}$ mice and in OPCs after Rgs12 deletion, whereas application of pertussis toxin (PTX) or overexpression of Rgs12 could rescue the defective OB differentiation via restoration of ERK phosphorylation. Our findings reveal that Rgs12 is an important regulator during osteogenesis and highlight Rgs12 as a potential therapeutic target for bone disorders. © 2018 American Society for Bone and Mineral Research.

KEY WORDS: OSTEOBLASTS; RGS12; CALCIUM CHANNEL/OSCILLATION; GAI SIGNALING

Introduction

Bone homeostasis intimately relies on the balance between bone-forming osteoblasts (OBs) and bone-degrading osteoclasts (OCs).[1,2] Any dysfunctional bone formation relative to bone resorption leads to defective skeletal integrity.[3,4] In contrast to antiresorptive treatment for bone diseases due to excessive bone resorption, bone disorders such as skeletal dysplasias or osteogenic bone tumors (too much or disorganized bone formation), and chronic kidney disease (CKD) or aging (reduced bone formation) are more challenging to treat because of the limited number of reliable drugs promoting osteogenesis and activity.[5–8] Therefore, uncovering potential therapeutic targets that regulate OB differentiation and function during skeletal development and remodeling remains an important objective for skeletal restoration.[7]

OBs are mononucleated cells derived from mesenchymal stem cell (MSC) lineage in the bone marrow and are uniquely

Received in original form May 29, 2018; revised form November 13, 2018; accepted November 17, 2018. Accepted manuscript online November 29, 2018.
Address correspondence to: Shuying (Sheri) Yang, MD, PhD, Department of Anatomy and Cell Biology, School of Dental Medicine, University of Pennsylvania, 240 South 40th Street, Levy 437, Philadelphia, PA 19104-6030, USA. E-mail: shuyingy@upenn.edu
*ZL, TL, and AG contributed equally to this work.
Additional Supporting Information may be found in the online version of this article.
Journal of Bone and Mineral Research, Vol. xx, No. xx, Month 2018, pp 1–13
DOI: 10.1002/jbmr.3645

responsible for bone formation.[2,9] The speed and effectiveness of OB precursor cells (OPCs) differentiating into mature OBs determines the rate of bone formation and is dependent on the expression of OB-specific transcription factors such as runt-related transcription factor 2 (Runx2) and osterix (Osx), followed by the expression of alkaline phosphatase (ALP) and secretion of extracellular matrix including type 1 collagen (Col1α1) and noncollagenous proteins, leading to the deposition and mineralization of bone matrix.[2,5,10] Calcium (Ca^{2+}) oscillations play an indispensable role during these processes through controlling gene expression and affecting OB differentiation and proliferation via Ca^{2+} signaling.[9,11–13] The excitability of Ca^{2+} signaling is determined by the contribution of extracellular Ca^{2+} influx, the effect of inositol 1, 4, 5-trisphosphate (IP3) to release Ca^{2+} from the endoplasmic reticulum (ER), and the capacity of removing Ca^{2+} from the cytosol by sarcoplasmic/endoplasmic reticulum Ca^{2+} ATPase pump (SERCA) and plasma membrane Ca^{2+} ATPase (PMCA).[12,14,15] Ca^{2+} channels such as voltage-sensitive Ca^{2+} channels (VSCCs) are involved in these Ca^{2+} signaling activities.[15–17] Studies showed that elevated intracellular Ca^{2+} through L-type Ca^{2+} channel (LTCC)-mediated Ca^{2+} influx, could lead to the activation of the extracellular signal-related protein kinase (ERK) signaling that is critical for OB differentiation and survival.[10,17–19] However, it remains largely unknown which factor(s) trigger and maintain Ca^{2+} oscillations in OBs and how Ca^{2+} signaling regulates OB differentiation via Ca^{2+} channels.

Regulators of G-protein signaling (Rgs) 12 (Rgs12) is the largest protein in the Rgs family with its multidomain architecture.[9,20] It possesses a PSD-95/Dlg/ZO-1 (PDZ) domain and a phosphotyrosine-binding (PTB) domain that are capable of binding the C terminus of G protein–coupled receptors (GPCRs) and interact with GPCR chemokine receptors, respectively, a conserved Rgs domain that is responsible for the GTPase accelerating protein (GAP) activity, a pair of Ras-binding domains (RBDs) that allows Rgs12 to integrate both heterotrimeric and monomeric G proteins signaling, and a single Gαi/o-Loco (GoLoco) motif that carries guanine nucleotide dissociation inhibitor (GDI) activity toward Gαi subunits, exclusively with Gαi1, Gαi2, and Gαi3, but not Gαs, Gαq, and Gαo.[9,20–22] This multidomain structure provides Rgs12 with the potential to modulate multiple signaling pathways,[9] including the signaling mediated by Gi-coupled GPCR, which has been reported to lead to the osteopenia phenotype through the transgenic expression of a constitutively active Gi-coupled GPCR in OBs.[23] Our previous studies revealed that Rgs12 plays an essential role in osteoclastogenesis through the regulation of PLCγ-Ca^{2+} channel-Ca^{2+} oscillations–nuclear factor of activated T cells 2 (NFAT2) pathways.[24–26] Loss of Rgs12 impaired Ca^{2+} oscillations and reduced NFAT2 expression in OCs, leading to the failure in OC differentiation and function.[24,26] However, the role of Rgs12 in OB differentiation and function, and how Ca^{2+} oscillations and signaling regulate these processes, is poorly understood.

In this study, we generated the OB-specific knockout of Rgs12 in mice that exhibited low bone mass, resulting in an osteopenia phenotype, and targeted deletion of Rgs12 in OPCs impaired OB differentiation and function through the disruption of Ca^{2+} channel/oscillations and Gαi-ERK signaling. Further, by treating with pertussis toxin (PTX), a Gi-specific inhibitor, or over-expressing Rgs12 in Rgs12-deficient OPCs, the defective OB differentiation ability was recovered, and these recoveries may attributed to the PTX or Rgs12 overexpression-induced ERK activation. Therefore, we conclude that Rgs12 is required for OB differentiation and function, and highlight Rgs12 as a potential therapeutic target for bone disorders.

Materials and Methods

Reagents, antibodies, and primers

All reagents, antibodies, and primers, as well as experimental protocols related to gene transfer, cell differentiation, and immunological and histological analysis, are listed in the Supporting Materials and Methods.

Generation of Rgs12 conditional knockout mice

Methodologies for generation of homozygous $Rgs12^{fl/fl}$ and Osx-Cre mice on C57BL/6J backgrounds have been described.[24,27] To specifically inactivate Rgs12 in the OB lineage, we crossed $Rgs12^{fl/fl}$ mice with Osx-Cre transgenic mice (OSX1-GFP::Cre) to generate Osx; $Rgs12^{fl/+}$ progeny, which were used for subsequent mating to produce heterozygous $Osx^{Cre/+}$; $Rgs12^{fl/fl}$ mice. Because the phenotype in $Rgs12^{fl/fl}$ mice were indistinguishable from that in Osx-Cre mice ($Osx^{Cre/+}$; $Rgs12^{+/+}$) after the age of 12 weeks, $Rgs12^{fl/fl}$ mice from the same litter of $Osx^{Cre/+}$; $Rgs12^{fl/fl}$ were used as control.[28–31] All mice were maintained in C57BL/6J background and housed maximally at five per cage under a standard 12-hour light/12-hour dark cycle condition and had free access to water and rodent diet. Once they reached 12 weeks old, qualified mice (average body shape and body weight) were randomized in each group according to their genotyping (see Supporting Materials and Methods). Both genders were used to include potential variation related to gender. All experiments using mice were performed following protocols and approved by the Institutional Animal Care and Use Committee (IACUC) of the State University of New York (Buffalo, NY) and the University of Pennsylvania.

Primary OPC culture, virus infection, and differentiation

Primary OPCs were isolated from the calvarial bone of $Rgs12^{fl/fl}$ mice at postnatal day 4 (four pups of either gender) according to a serial digestion method as previously performed.[27] In brief, calvarial bone was dissected, fragmented, and subjected to sequential digestions in collagenase type I and 0.25% trypsin. Cells from this digestion were plated in complete culture medium (α-MEM, 10% FBS, penicillin, and streptomycin) at 37°C in a humidified 5% CO_2 atmosphere. Upon reaching 90% of confluence, cells were trypsinized, reseeded, and cultured for further experiments. OPCs from $Rgs12^{fl/fl}$ mice were infected with adenovirus (Ad-Cre, Ad-Null, or Ad-GFP), Ad-Cre infection yielded an approximate 85% deletion of Rgs12 in $Rgs12^{fl/fl}$ OPCs, which were labeled as $Rgs12^{d/d}$. Ad-Null–treated or Ad-GFP–treated cells were used as control and marked as $Rgs12^{f/f}$; Ad-Null–treated cells were specially used in Ca^{2+} imaging experiments. For osteogenic differentiation, OPCs were treated with osteogenic medium (OS medium), composed of complete culture medium with addition of β-glycerophosphate, ascorbic acid, and dexamethasone. For experiments evaluating Gα signaling, PTX (100 ng/mL; Thermo Fisher Scientific, Waltham, MA, USA) was also added to the OS medium.[32]

Quantitative real-time PCR

Quantitative real-time PCR (qPCR) was carried out as described, with slight modifications.[27,33] In brief, total RNA was extracted using Trizol and quantified by NanoDrop™ 2000 (Thermo Fisher Scientific). cDNA was synthesized from 2 μg of total RNA, and

PCR amplifications were performed in triplicate with SYBR Green qPCR Master Mix (Bimake.com, Houston, TX, USA) on CFX96 real-time PCR machine (Bio-Rad Laboratories, Hercules, CA, USA) using the following steps: 95°C for 5 min, 40 cycles of 95°C for 15 s, and 60°C for 30 s. Gene expression were calculated using the delta-delta comparative threshold cycle algorithm ($2^{-\Delta\Delta CT}$) method and normalized to housekeeping gene GAPDH. Primer sequences are listed in Supporting Table 1 and validation results are shown in Supporting Fig. 3.

Bone micro–computed tomography analysis

A quantitative analysis of the femur morphology and micro-architecture was performed using a micro–computed tomography (μCT) system (Micro-CT 35; Scanco Medical AG, Brüttisellen, Switzerland) as described by de Bakker and colleagues[34] and Chandra and colleagues.[35] Femurs from 12-week-old $Osx^{Cre/+}$; $Rgs12^{+/+}$, $Rgs12^{fl/fl}$ and $Osx^{Cre/+}$; $Rgs12^{fl/fl}$ mice of either gender ($n = 3$ per gender, $n = 6$ in total of each group) were fixed with 4% (wt/vol) paraformaldehyde (PFA) for 24 hours, rinsed with PBS, and scanned. The distal end of the femur corresponding to a 0-mm to 6.9-mm region and the whole skull were scanned at 10.5 μm isotropic voxel size (μm^3) to acquire 10.5 μm resolution per scan, with 300 ms integration time, 145 μA current, and 55 kVp energy. All images were first smoothed by a Gaussian filter (sigma = 1.2, support = 2) and a global threshold corresponding to 544 mg hydroxyapatite (HA)/cm^3 for trabecular and calvarial bone, 709 mg HA/cm^3 for cortical bone. The trabecular and cortical bone architecture were assessed at the distal femoral metaphysis and midshaft. Two hundred (200) slices (2 mm) above the highest point of the growth plate were contoured for trabecular bone analysis, including the percentage of bone volume (BV/TV, %), trabecular number (Tb.N, mm^{-1}), trabecular thickness (Tb.Th, mm), and trabecular spacing (Tb.Sp, mm). Fifty (50) slices (0.5 mm) of the femur midshaft were contoured for cortical bone analysis, including the cortical area (Ct.Ar, mm^2), total area (Tt.Ar, mm^2), cortical area fraction (Ct.Ar/Tt.Ar, %), and cortical thickness (Ct.Th, mm). Four hundred (400) slices of calvarial bone above the middle joint point of the frontal and parietal bone were contoured for calvarial BV/TV.

In situ detection of apoptotic cells

Terminal deoxynucleotidyl transferase-mediated dUTP-biotin nick-end labeling (TUNEL) assay (In Situ Cell Death Detection Kit, TMR red; Sigma-Aldrich, St. Louis, MO, USA) was performed as described.[36] In brief, sections were permeabilized with 0.1% Triton X-100, then incubated with TUNEL reaction mixture (label solution and enzyme solution) for 1 hour at 37°C avoiding light. After rinsing the sections three times in PBS for 5 min, the nuclei were counterstained with 4,6-diamidino-2-phenylindole (DAPI) and mounted. Images were acquired using the Leica fluorescent microscope (DMI6000B; Leica, Wetzlar, Germany). TUNEL-positive cells and total nuclei (DAPI staining) on cortical and trabecular bones were counted and analyzed.

Ca^{2+} imaging

Measurements of Ca^{2+} oscillation were performed as described with slight modification.[24,37] OPCs after Ad-Null or Ad-Cre infection were reseeded at a density of 2×10^5 cells/35-mm dish and induced with OS medium for 3 days. Then, cells were loaded with 5μM fluo-4 AM (Thermo Fisher Scientific) for 50 min in complete culture medium containing 0.05% Pluronic F127 (Sigma), washed, and incubated in Hank's Balanced Salt Solution (HBSS). Change of intracellular Ca^{2+} concentration was accessed by a Leica fluorescent microscope (DMI6000B; Leica) with excitation wavelength at 488 nm and emission wavelength at 505 to 530 nm. Signals were recorded simultaneously at 5-s intervals for 30 min, and fluorescence intensity was analyzed using Leica Application Suite X (Leica) software and plotted over time.

To measure intracellular Ca^{2+} concentration change during extracellular Ca^{2+} influx or release from ER in OPCs, cells were washed and incubated a in Ca^{2+}-free isotonic solution (ISO) (see Supporting Materials and Methods) after fluo-4 AM loading. Change of intracellular Ca^{2+} concentration was accessed and recorded for 45 min as mentioned in the first paragraph of section Ca^{2+} imaging. Once the cells reached a stable baseline level of cytosolic Ca^{2+}, the Ca^{2+}-free ISO was exchanged for a Ca^{2+}-free ISO containing 1μM TG (Sigma-Aldrich) to trigger Ca^{2+} release from the ER, a normal ISO containing 1.3mM $CaCl_2$ to induce extracellular Ca^{2+} influx, or a normal ISO containing 10μM Bay K8644 (Sigma) to induce L-type Ca^{2+} channel amplified influx.[17,37] Changes of intracellular Ca^{2+} intensity were normalized by the initial Ca^{2+} level of cell itself.

GTPase assay

GTPase activity was performed according to the manufacturer's instructions (602-0120; Innova Biosciences, San Diego, CA, USA).[38] In brief, GTPase activity of OPCs was measured based on hydrolysis of guanosine triphosphate (GTP) to guanosine diphosphate (GDP) and inorganic phosphorous by adding PiColorLock™ Gold substrate (Innova Biosciences) to cell protein extract. Colorimetric measurements were read at the wavelength of 635 nm and GTPase activities were assessed on the basis of inorganic complex solutions.

Statistical analysis

The number of animals in each group was calculated to detect a 50% difference at alpha = 0.05 and power = 0.8 using Graphpad StatMate 2.0 software (GraphPad Software, San Diego, CA, USA). All data are presented as mean ± standard deviation (SD) ($n > 3$) and analyzed by using unpaired, two-tailed Student's t test for the comparison between two groups or one-way ANOVA followed by Sidak's multiple comparison test for grouped samples. Values of $p < 0.05$ were considered to be significant. Graphpad Prism 6.0 software (GraphPad Software) was used to perform statistical analysis.

Results

Rgs12 was expressed in murine OBs and gradually increased throughout osteogenesis

To evaluate Rgs12 expression in different tissues and bone cells, samples from multiple organs, precursor cells (OB from calvarial bone and OC from bone marrow macrophages) were isolated from WT mice, and cells were continuously differentiated for 7 days before test. Western blot (WB) showed Rgs12 protein to be highly expressed in brain and lung, with a lower expression level in bone (Fig. 1*A*). However, OBs exhibited more Rgs12 expression than OCs (Fig. 1*B*). Further, to monitor Rgs12 expression pattern during osteogenesis, OPCs were harvested at indicated time points (days 0, 3, 7, and 14) of OS medium stimulation. The mRNA level of Rgs12 was gradually increased and significantly boosted after day 7 of osteogenesis (Fig. 1*C*).

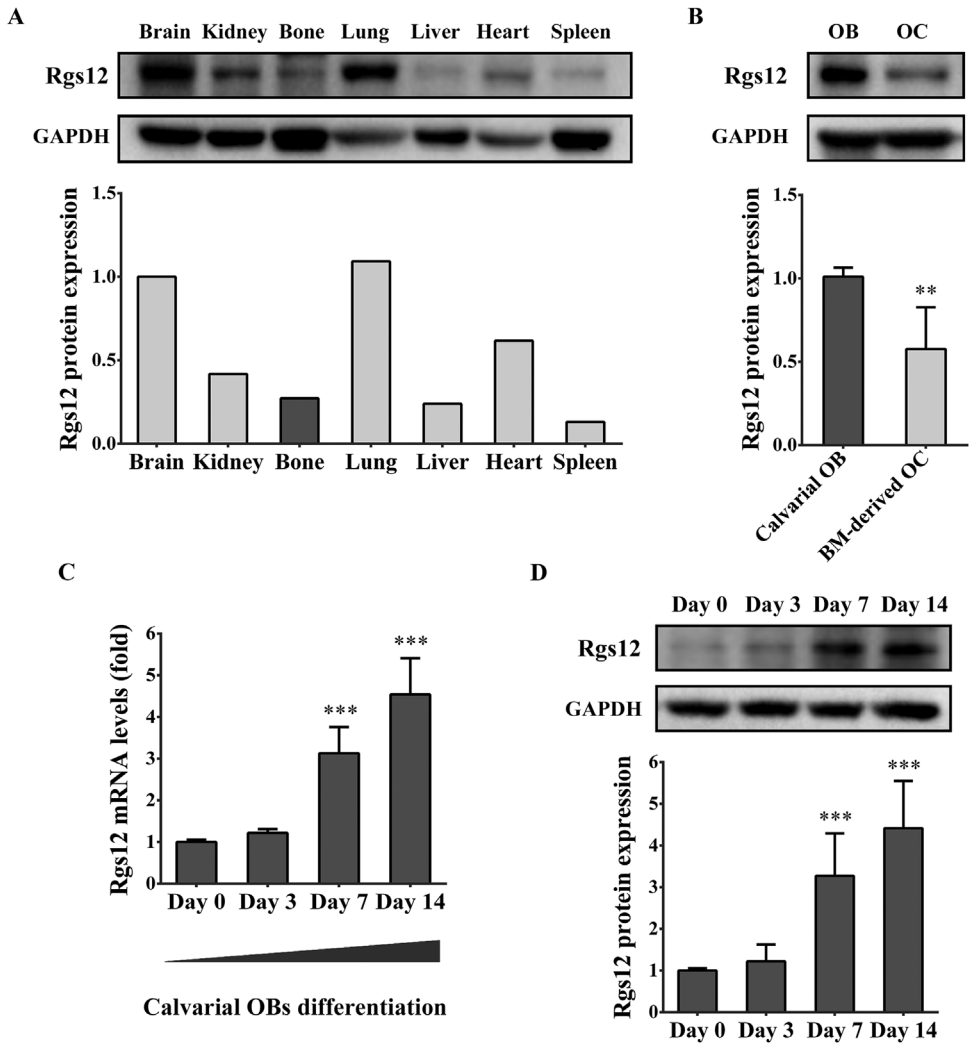

Fig. 1. Rgs12 is expressed in murine bone tissue and OBs, with expression increases during osteogenesis. (*A*) WB showed Rgs12 protein expression in multiple organs of WT mice. (*B*) Rgs12 protein expression in OBs and OCs. Precursors were derived from calvarial bone (for OBs) or BM macrophages (for OCs) of WT mice and differentiated for 7 days. $^{**}p < 0.01$ versus OBs. (*C*) qPCR showed Rgs12 mRNA level of calvarial OPCs increased with OS medium stimulation by day. (*D*) qPCR results were confirmed at protein level, $^{***}p < 0.001$ versus day 0, $n = 4$. All quantitative data were normalized to GAPDH and are presented as mean ± SD. BM = bone marrow; OB = osteoblast; OC = osteoclast; OPC = OB precursor; OS medium = osteogenic medium; WT = wild-type.

The protein level demonstrated a similar result (Fig. 1*D*) and further indicated a correlation between Rgs12 and osteogenesis.

Targeted deletion of Rgs12 in OPCs reduced bone mass with decreased OB number and increased apoptotic cells population

To better understand the role of Rgs12 during osteogenesis in vivo, we generated Rgs12 conditional knockout (CKO) mice ($Osx^{Cre/+}$; $Rgs12^{fl/fl}$ mice) and $Osx^{Cre/+}$; $Rgs12^{fl/fl}$ mice were born with expected Mendelian ratios. Deletion of Rgs12 was examined using genomic DNA from calvarial bone (Supporting Fig. 1A). Low levels of Rgs12 mRNA (Supporting Fig. 1B) and significantly diminished expression of Rgs12 protein were found in calvarial bone of $Osx^{Cre/+}$; $Rgs12^{fl/fl}$ mice (Supporting Fig. 1C). In addition, expression of Rgs12 was significantly reduced in femur sample of $Osx^{Cre/+}$; $Rgs12^{fl/fl}$ mice (Supporting Fig. 1D), indicating a successful generation of knockout model.

To assess whether deletion of Rgs12 affects bone physiology, femurs from 12-week-old mice were evaluated by μCT analysis. With a marked reduction in trabecular bone (Fig. 2*A*, upper panel), the percentages of BV/TV, Tb.N, and Tb.Th in $Osx^{Cre/+}$; $Rgs12^{fl/fl}$ mice were 41%, 64%, and 78% of those in $Rgs12^{fl/fl}$ mice, whereas Tb.Sp increased to 160% (Fig. 2*B*). Cortical bone parameters also reflected a reduced tendency in $Osx^{Cre/+}$; $Rgs12^{fl/fl}$ mice, as the percentages of Ct.Ar, Tt.Ar, Ct.Ar/Tt.Ar, and Ct.Th were 77%, 80%, 96%, and 83% of those in $Rgs12^{fl/fl}$ mice (Fig. 2*A*, lower panel, *C*), indicating an osteopenia phenotype. $Osx^{Cre/+}$; $Rgs12^{+/+}$ showed no significant difference in both trabecular and cortical bone compared with $Rgs12^{fl/fl}$ mice at this age as reported,[28–31] indicating the $Rgs12^{fl/fl}$ mice from the same litter of $Osx^{Cre/+}$; $Rgs12^{fl/fl}$ could also be used as qualified

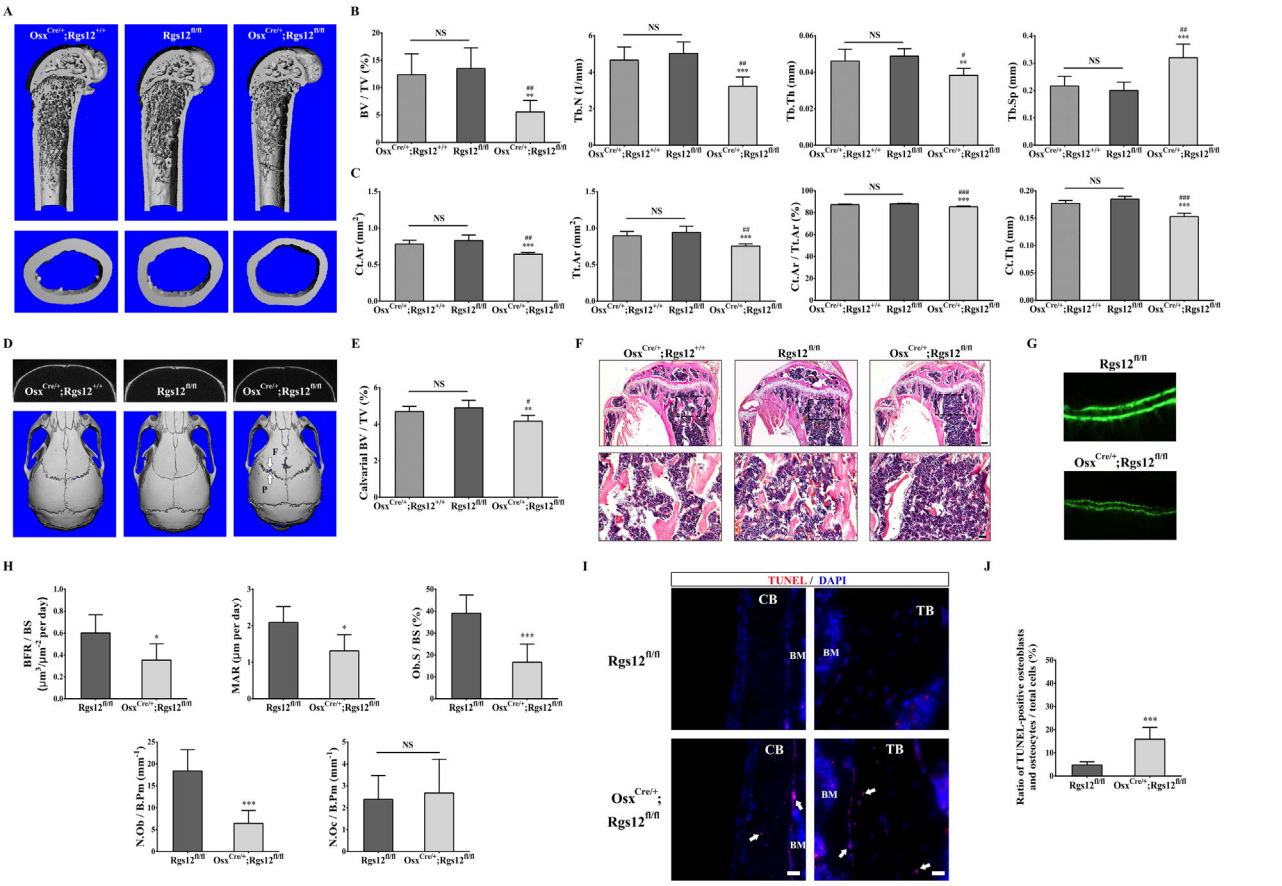

Fig. 2. Deletion of Rgs12 in OPCs ($Osx^{Cre/+}$; $Rgs12^{fl/fl}$) causes significant osteopenia with reduced OB formation and increased apoptotic cells. (*A*) μCT analysis of the femurs from 12-week-old $Osx^{Cre/+}$; $Rgs12^{+/+}$, $Rgs12^{fl/fl}$, and $Osx^{Cre/+}$; $Rgs12^{fl/fl}$ mice (upper panel, longitudinal view of metaphyseal region; lower panel, axial view of cortical bone). (*B*) Quantitative analysis of the BV/TV, Tb.N, Tb.Th, and Tb.Sp of samples shown in *A*. (*C*) Quantitative analysis of Ct.Ar, Tt.Ar, Ct.Ar/Tt.Ar, and Ct.Th of samples shown in *A*. (*D*) μCT analysis of calvaria bone from the same mice. Upper panel: representative coronal μCT image of each group. Lower panel: 3D overview, arrowheads indicate coronal sutural area. (*E*) Quantitative analysis of calvarial BV/TV. $^{**}p < 0.01$, $^{***}p < 0.001$ versus $Rgs12^{fl/fl}$ mice, $\#p < 0.05$, $\#\#p < 0.01$, $\#\#\#p < 0.001$ versus $Osx^{Cre/+}$; $Rgs12^{+/+}$ mice, $n = 6$. (*F*) H&E staining of the proximal tibia metaphyseal regions. Lower panel: higher magnification. Scale bars = 200 μm (upper) or 50 μm (lower). (*G*) Dynamic histomorphometry of tibia after double calcein labeling. (*H*) Quantitative analysis of BFR/BS, MAR, Ob.S/BS, N.Ob/B.Pm, and N.Oc/B.Pm from double calcein labeling. (*I*) Merged images of apoptotic cells (red, TUNEL-labeling) and total cells (blue, DAPI-labeling) in CB and TB. Arrowheads indicated the apoptotic OBs. Scale bar = 50 μm (left) or 25 μm (right). (*J*) Percentage of TUNEL-positive OBs and OCs per total cells in the bone area shown in *I*. $^{*}p < 0.05$, $^{***}p < 0.001$, or NS versus $Rgs12^{fl/fl}$ mice, $n = 6$. Quantitative data are presented as mean ± SD. BFR/BS = bone formation rate per bone surface; BM = bone marrow; BV/TV = percentage of bone volume; CB = cortical bone; Ct.Ar = cortical area; Ct.Ar/Tt.Ar = cortical area fraction; Ct.Th = cortical thickness; F = frontal bone; MAR = mineral apposition rate; N.Ob/B.Pm = OB number per bone perimeter; N.Oc/B.Pm = OC number per bone perimeter; NS = not statistically significant; Ob.S/BS = OB surface per bone surface; P = parietal bone; TB = trabecular bone; Tb.N = trabecular number; Tb.Sp = trabecular separation; Tb.Th = trabecular thickness; Tt.Ar = total area.

controls in long-bone study. In calvarial bone, although coronal sutural area was still slightly unclosed in $Osx^{Cre/+}$; $Rgs12^{+/+}$ mice, the frontal and parietal bone exhibited bone mass similar to the $Rgs12^{fl/fl}$ mice (Fig. 2*D*, *E*). Contrarily, $Osx^{Cre/+}$; $Rgs12^{fl/fl}$ mice showed obvious calvarial defects in both sutural area and bone mass (Fig. 2*D*, *E*). H&E staining on tibias also exhibited dramatically decreased trabecular bone in $Osx^{Cre/+}$; $Rgs12^{fl/fl}$ mice (Fig. 2*F*). In addition, dynamic histomorphometric analysis of $Osx^{Cre/+}$; $Rgs12^{fl/fl}$ mice showed a significant reduction in bone formation rate per bone surface (BFR/BS), mineral apposition rate (MAR), OB surface per bone surface (Ob.S/BS), and OB number per bone perimeter (N.Ob/B.Pm) (Fig. 2*G*, *H*); no change was found in OC number per bone perimeter (N.Oc/B.Pm) compared with $Rgs12^{fl/fl}$ mice (Fig. 2*H*). We further identified whether cell apoptosis contributed to the reduction of BFR and OB number. Surprisingly, TUNEL-positive apoptotic OBs and osteocytes increased 3.2-fold in $Osx^{Cre/+}$; $Rgs12^{fl/fl}$ mice, and both cortical and trabecular bone of femur were affected (Fig. 2*I*, *J*). All these data suggested an osteopenia phenotype caused by impaired osteogenesis process after Rgs12 deletion.

Deletion of Rgs12 impairs OB proliferation and differentiation

To further determine whether the decreased bone mass in $Osx^{Cre/+}$; $Rgs12^{fl/fl}$ mice resulted from deficient OBs, we investigated the role of Rgs12 in OB differentiation and function in vitro. OPCs were isolated from $Rgs12^{fl/fl}$ mice and infected

with different adenovirus as described in the Materials and Methods. qPCR result showed Ad-Cre infection yielded an approximate 85% reduction of Rgs12 in Rgs12$^{fl/fl}$ OPCs, whereas Ad-GFP and Ad-Null infection had no reduced effects of Rgs12 in OPCs (Fig. 3*A*). Because of the increase of TUNEL-positive apoptotic OBs and osteocytes in Osx$^{Cre/+}$; Rgs12$^{fl/fl}$ mice (Fig. 2*I*, *J*), we first investigated whether cell viability was affected after Rgs12 deletion. Interestingly, under normal cell passage conditions, deletion of Rgs12 in OPCs apparently impaired cell viability during osteogenic induction (Supporting Fig. 2A); however, under cell confluency conditions, no significant change of cell viability was found (Supporting Fig. 2B), suggesting a limited effect on cell proliferation after Rgs12 deletion.

Then, we examined the deletion effect on OB differentiation, and all differentiation-related experiments were performed under cell confluency conditions to eliminate proliferation factors (Supporting Fig. 2B). Deletion of Rgs12 in OPCs impaired OB differentiation dramatically, evidenced by lower expression level of OB differentiation markers, including ALP, Col1α1, osteocalcin (OCN), and Runx2, after 7 days of osteogenic induction (Fig. 3*B*). These impairments were also confirmed by reduced expression of extracellular matrix proteins Col1 and OCN (Fig. 3*C*). In addition, defective OB differentiation and mineralization were detected in Rgs12$^{d/d}$ OBs by exhibiting less ALP activity (Fig. 3*D*, *F*) and reduced bone nodule formation (Fig. 3*E*, *F*).

Deletion of Rgs12 inhibited GTPase activity and Ca^{2+} oscillations, blocking ERK activation in OBs, and application of PTX could rescue defective OB differentiation

Studies showed that signaling mediated by Gi-coupled GPCR served as a negative regulator of OB differentiation,[9,23,39] whereas Rgs12 acted as an antagonist of this signaling via enhancing GTPase activity toward the Gαi subunit.[9,20] Therefore, we compared the differences of GTPase activities and cAMP level between Rgs12$^{f/f}$ and Rgs12$^{d/d}$ OPCs. Our result showed that Pi released in Rgs12$^{d/d}$ OPCs was only 53% of that in Rgs12$^{f/f}$ OPCs (Fig. 4*A*) and cAMP level also reduced in Rgs12$^{d/d}$ OPCs after OS medium stimulation (Fig. 4*B*), indicating a possible enhanced Gαi-mediated signaling in Rgs12$^{d/d}$ OPCs. Accumulating studies showed that Gαi-mediated signaling could crosstalk with Ca^{2+} signaling to regulate downstream cAMP via Ca^{2+} oscillations[40,41]; our previous study showed that Rgs12 regulates Ca^{2+} oscillations during OC differentiation.[24] Thus, we hypothesized Rgs12 is also required for Ca^{2+} oscillations during OB differentiation. By monitoring intracellular Ca^{2+} change in OPCs after OS medium stimulation for 3 days, we found a sustained frequency of Ca^{2+} oscillations at approximately 2 min per interval in the Rgs12$^{f/f}$ cells (Fig. 4*C*, left panel); however, in Rgs12$^{d/d}$ cells, Ca^{2+} oscillations were barely detectable (Fig. 4*C*, right panel). To further confirm the involvement of Rgs12 in these two pathways, phosphorylated ERK (p-ERK), the downstream mediator of both pathways, was examined.[18–20,42] Reduced expression of p-ERK was found in OBs of Osx$^{Cre/+}$; Rgs12$^{fl/fl}$ mice (Fig. 4*D*, *E*), and also showed in Rgs12$^{d/d}$ cells after OS medium stimulation (Fig. 4*F*), suggesting a more common inactive status of OBs after Rgs12 deletion. PTX was then applied to purposely feedback the role of Rgs12 in Gαi-mediated signaling during OB differentiation. As expected, application of PTX displayed a rescue of ALP activity in Rgs12$^{d/d}$ OBs (Fig. 4*G*), and further results showed p-ERK was significantly upregulated in PTX-treated Rgs12$^{d/d}$ cells (Fig. 4*H*). These findings supported the regulator role of Rgs12 in OB differentiation through Gαi-mediated ERK signaling.

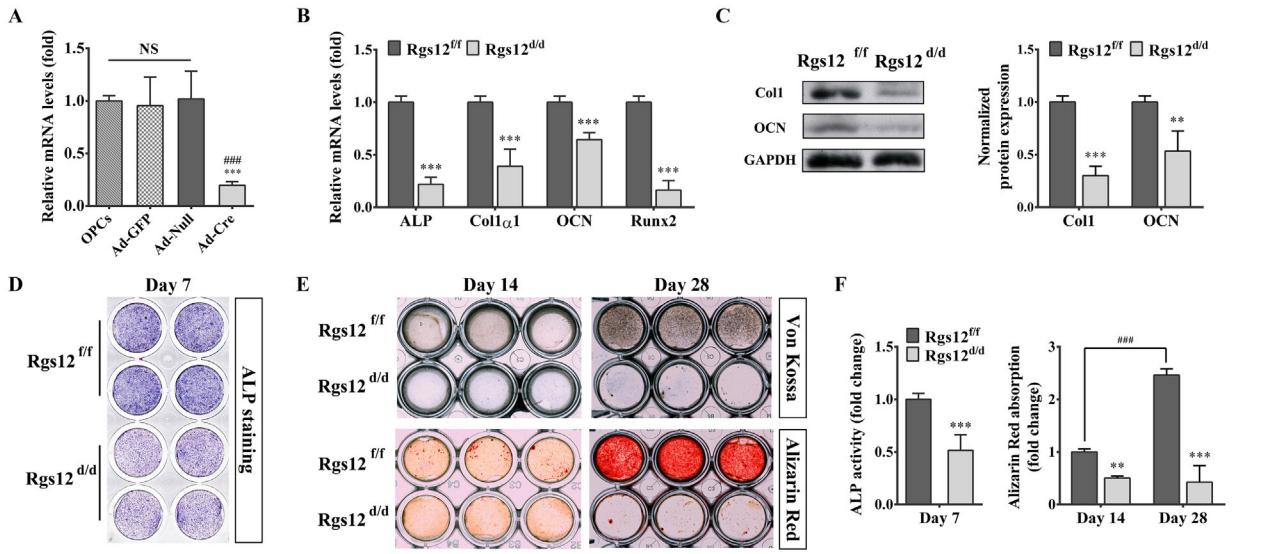

Fig. 3. Deletion of Rgs12 impairs OB differentiation. (*A*) Rgs12 mRNA level in OPCs after adenovirus infection, normalized to GAPDH ($n = 6$). $^{***}p < 0.001$ versus Ad-GFP; $###p < 0.001$ versus Ad-Null; NS, not statistically significant between groups. (*B*) qPCR analysis of OB marker genes ALP, Col1α1, OCN, and Runx2 in OPCs at day 7 of osteogenic induction. Rgs12$^{f/f}$: OPCs from Rgs12$^{fl/fl}$ mice infected with Ad-GFP or Ad-Null; Rgs12$^{d/d}$: infected with Ad-Cre. $^{***}p < 0.001$ versus control, $n = 4$. (*C*) WB analysis of extracellular matrix proteins at day 7 of osteogenic induction. $^{**}p < 0.01$, $^{***}p < 0.001$ versus control, $n = 4$. (*D*) Representative images of ALP staining. (*E*) Representative images of Von Kossa and Alizarin Red staining. (*F*) ALP activity and Alizarin Red absorption of OPCs at indicated days of osteogenic induction. $^{**}p < 0.01$, $^{***}p < 0.001$ versus Rgs12$^{f/f}$ cells; $###p < 0.001$ versus Rgs12$^{f/f}$ cells at day 14 of osteogenic induction; $n = 4$. Data are presented as mean ± SD.

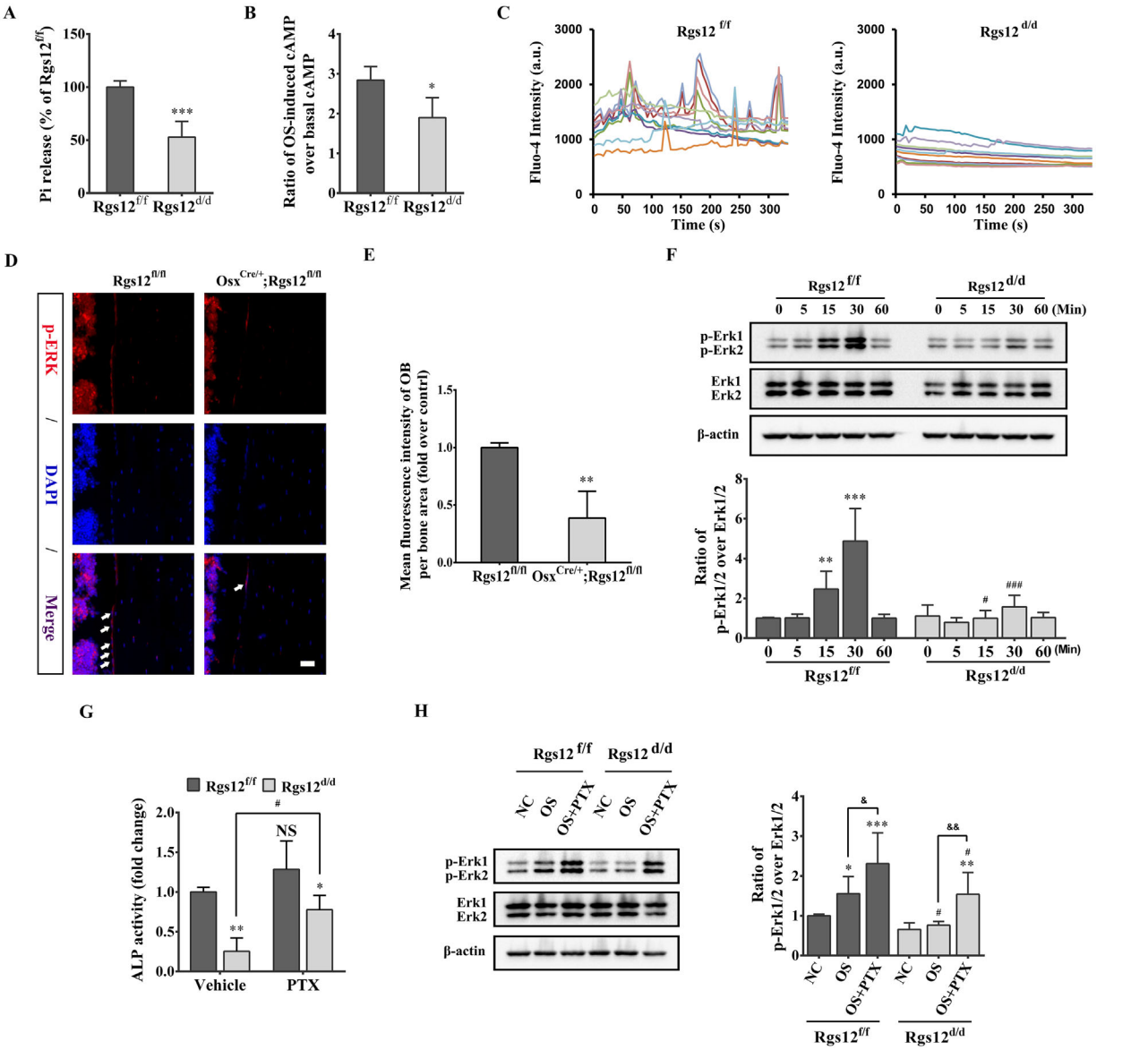

Fig. 4. Deletion of Rgs12 inhibits GTPase activity, Ca^{2+} oscillations and sequentially blocks ERK activation; and PTX treatment could rescue defective OB differentiation. (*A*) GTPase assay showed Pi release level in OPCs. (*B*) ELISA showed intracellular cAMP of OPCs in response to OS medium stimulation. Cells were starved for 6 hours prior to OS medium stimulation or completed medium stimulation (basal cAMP) for 30 min. $^{*}p < 0.05$, $^{***}p < 0.001$ versus $Rgs12^{f/f}$ cells; $n = 4$. (*C*) Ca^{2+} oscillations in OPCs after 3 days of osteogenic induction. Cells were traced, calculated, and plotted over time using different colors ($n = 10$ cells of each group). (*D*) Representative images of IF with primary p-ERK antibody counterstained with DAPI; arrowheads indicated OBs in phosphorylated status. Scale bar = 25 μm. (*E*) Quantitative analysis of mean fluorescence intensity of OBs per mean fluorescence intensity of bone area shown in *D*. $^{**}p < 0.01$ versus $Rgs12^{fl/fl}$ mice, $n = 4$. (*F*) WB showed p-ERK expression in OPCs. Cells were starved for 6 hours prior to OS medium stimulation, normalized to total ERK. $^{**}p < 0.01$, $^{***}p < 0.001$ versus 0 min; $\#p < 0.05$, $\#\#\#p < 0.001$ versus same time point in $Rgs12^{f/f}$ cells; $n = 4$. (*G*) ALP activity of OPCs with or without PTX treatment at day 7 of osteogenic induction. $^{*}p < 0.05$, $^{**}p < 0.01$ versus $Rgs12^{f/f}$ cells within groups; NS, not statistically significant or $\#p < 0.05$ versus same cells without PTX treatment; $n = 4$. (*H*) WB showed p-ERK in OPCs with or without PTX treatment. Cells in PTX group were pretreated with PTX (100 ng/mL) overnight in complete medium, followed by 6 hours starvation and then OS medium stimulation combined with PTX for 15 min. NC and OS group were only stimulated with OS medium for 0 or 15 min. $^{*}p < 0.05$, $^{**}p < 0.01$, $^{***}p < 0.001$ versus NC within groups; $\#p < 0.05$ versus same subgroup in $Rgs12^{f/f}$; $^{\&}p < 0.05$, $^{\&\&}p < 0.01$ versus OS within groups; $n = 4$. Data were presented as mean ± SD. cAMP = cyclic AMP; IF = immunofluorescence; NC = Negative control, OS medium stimulation for 0 min; p-ERK = phosphorylated ERK; Pi = inorganic phosphate.

Deletion of Rgs12 restrained the entry sources of cytosolic free Ca^{2+} in OPCs

Given that Ca^{2+} oscillations arise from periodic Ca^{2+} influx and repetitive release and reuptake of free Ca^{2+} from intracellular stores,[43,44] we investigated whether Rgs12 deletion affected Ca^{2+} entry from these two main sources. First, we determined the influence of Rgs12 on Ca^{2+} influx. The fluorescence intensity increased gradually in $Rgs12^{f/f}$ cells after normal ISO application, whereas elevating amplitude in $Rgs12^{d/d}$ cells decreased

dramatically (Fig. 5*A*, *B*; Supporting Videos 1 and 2). Significant differences between Rgs12$^{f/f}$ and Rgs12$^{d/d}$ cells occurred after 3 min of ISO application, and reached maximum after 13:10 min (Fig. 5*C*), indicating a restraint on Ca^{2+} entry to cytosol from the extracellular environment. Next, we determined whether deletion of Rgs12 also affected Ca^{2+} release from ER. To achieve that, cells were treated with 1μM TG to inhibit SERCA and unmask an endogenous leak for Ca^{2+}.[37,43] Similar to Ca^{2+} influx, elevating amplitude of ER Ca^{2+} release in Rgs12$^{d/d}$ cells decreased dramatically (Fig. 5*D*, *E*; Supporting Videos 3 and 4); significant differences were captured after 15 s of TG application and reached maximum level after 90 s (Fig. 5*F*). Collectively, these data suggested deletion of Rgs12 restrained both extracellular and intracellular entry sources of cytosolic free Ca^{2+}, leading to inhibition on Ca^{2+} oscillations in OPCs.

Deletion of Rgs12 attenuated the Bay K8644-amplified Ca^{2+} influx

LTCCs, via Ca^{2+} influx, play a key role in regulating intracellular Ca^{2+} homeostasis of OBs.[17,18] Thus, we used Bay K8644, an agonist of LTCCs, to determine whether LTCCs partly contribute to the restrain of Ca^{2+} influx after Rgs12 deletion.[45] First, Rgs12$^{f/f}$ OPCs were treated with or without 10μM Bay K8644 in normal ISO, to ensure an amplified Ca^{2+} influx induced by Bay K8644. Our results showed the fluorescence intensity of Bay K8644-treated cells increased immediately after Bay K8644 application (Fig. 6*A*, *B*; Supporting Videos 5 and 6) and reached significant differences after 30 s of application (Fig. 6*C*), showing an amplified Ca^{2+} influx via LTCCs. Next, we compared the effect of Bay K8644 on Rgs12$^{f/f}$ and Rgs12$^{d/d}$ cells; no obvious increasing signals were detected in Rgs12$^{d/d}$ cells after a limited and transient fluorescence peak induced by Bay K8644 application (Fig. 6*D*, *E*; Supporting Videos 7 and 8). Significant differences between Rgs12$^{f/f}$ and Rgs12$^{d/d}$ cells were even captured at logarithmic phase of fluorescence signals (Fig. 6*F*). These results confirmed the involvement of LTCCs in restraint of Ca^{2+} influx caused by Rgs12 deletion.

Ectopic expression of Rgs12 or constitutive ERK activation rescued defective OB differentiation

To test the potential therapeutic effect of Rgs12 on defective OBs, we ectopically expressed Rgs12 in Rgs12$^{d/d}$ OPCs. Successful Rgs12 overexpression was confirmed by WB (Fig. 7*A*, *B*). Overexpression of Rgs12 in Rgs12$^{d/d}$ OPCs exhibited a recovery on OS-induced cAMP level (Fig. 7*C*) and defective OB differentiation, evidenced by a significant improvement in ALP activity and bone nodule formation (Fig. 7*D*, *E*). Surprisingly, an enhanced effect on cAMP level and OB differentiation was observed in Rgs12$^{f/f}$ OPCs with overexpressed Rgs12 (Fig. 7*C*–*E*). Next, we identified whether constitutive activation of ERK in Rgs12$^{d/d}$ OPCs could also show the same rescue effect. Constitutive ERK activation was successfully detected in OPCs after MEK1^{DD} transfection as reported (Fig. 7*F*, *G*).[46,47] OB differentiation ability but not cAMP level was obviously improved after introducing ERK activation into Rgs12$^{d/d}$ OPCs (Fig. 7*H*–*J*), as well as the enhanced effect in Rgs12$^{f/f}$ OPCs. These

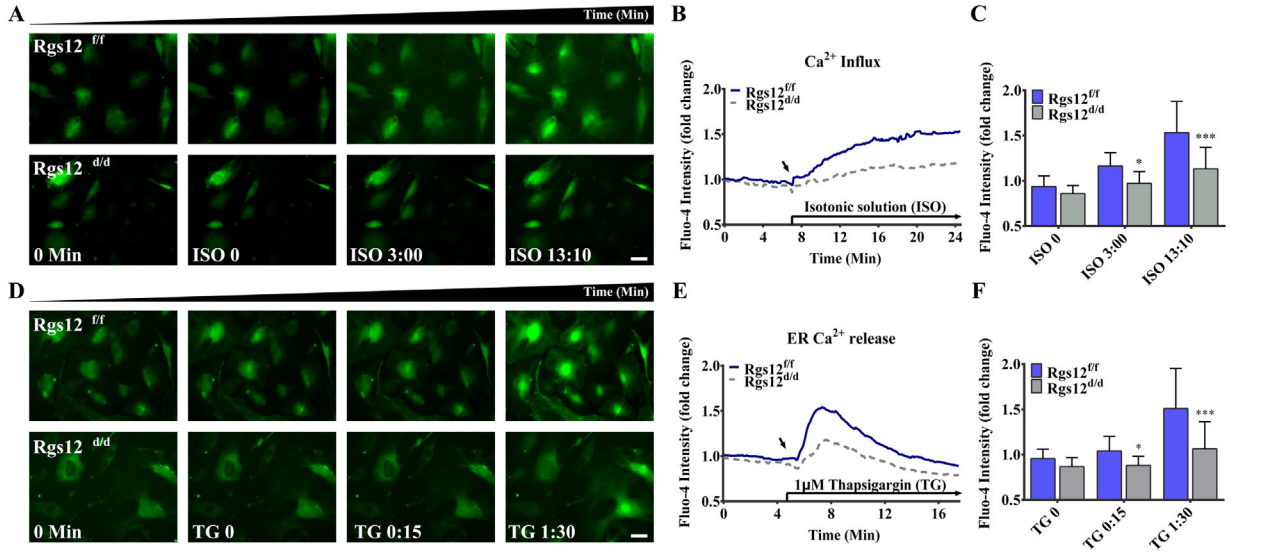

Fig. 5. Deletion of Rgs12 restrains Ca^{2+} entry from extracellular environment and intracellular ER store to the cytosol. (*A*–*C*) Ca^{2+} influx in Rgs12$^{f/f}$ or Rgs12$^{d/d}$ OPCs. (*A*) Representative images of intracellular Ca^{2+} in OPCs before (0 min) and after ISO (started from ISO 0 min) stimulation. OPCs were incubated in Ca^{2+}-free ISO to reach a stable baseline level of cytosolic Ca^{2+}, and then changed into normal ISO, which contains 1.3mM $CaCl_2$ to induce extracellular Ca^{2+} influx. Upper panel, Rgs12$^{f/f}$ OPCs; lower panel, Rgs12$^{d/d}$ OPCs. (*B*) Overlay of traces from OPCs. Arrow indicates the time point when extracellular Ca^{2+} presented. Data is expressed as a fold change of fluo-4 intensity, accomplished by normalizing each cell's fluorescence intensity to its initial intensity ($n = 39$ cells per group). (*C*) Quantitative analysis of fluo-4 intensity at indicated time point. $^{*}p < 0.05$, $^{***}p < 0.001$ versus Rgs12$^{f/f}$ cells. (*D*–*F*) ER Ca^{2+} release in Rgs12$^{f/f}$ or Rgs12$^{d/d}$ OPCs. (*D*) Representative images of intracellular Ca^{2+} in OPCs before (0 min) and after stimulation of 1μM TG (started from TG 0 min). OPCs were incubated in Ca^{2+}-free ISO to reach the baseline level of cytosolic Ca^{2+}, and then treated with TG in Ca^{2+}-free ISO to trigger Ca^{2+} release from the ER. Upper panel, Rgs12$^{f/f}$ OPCs; lower panel, Rgs12$^{d/d}$ OPCs. (*E*) Overlay of traces from OPCs. Arrow indicates the time point of TG application ($n = 47$ cells per group). (*F*) Quantitative analysis of fluo-4 intensity at indicated time point. $^{*}p < 0.05$, $^{***}p < 0.001$ versus Rgs12$^{f/f}$ cells. Scale bars = 50 μm. Quantitative data are presented as mean ± SD. ISO = isotonic solution; TG = thapsigargin.

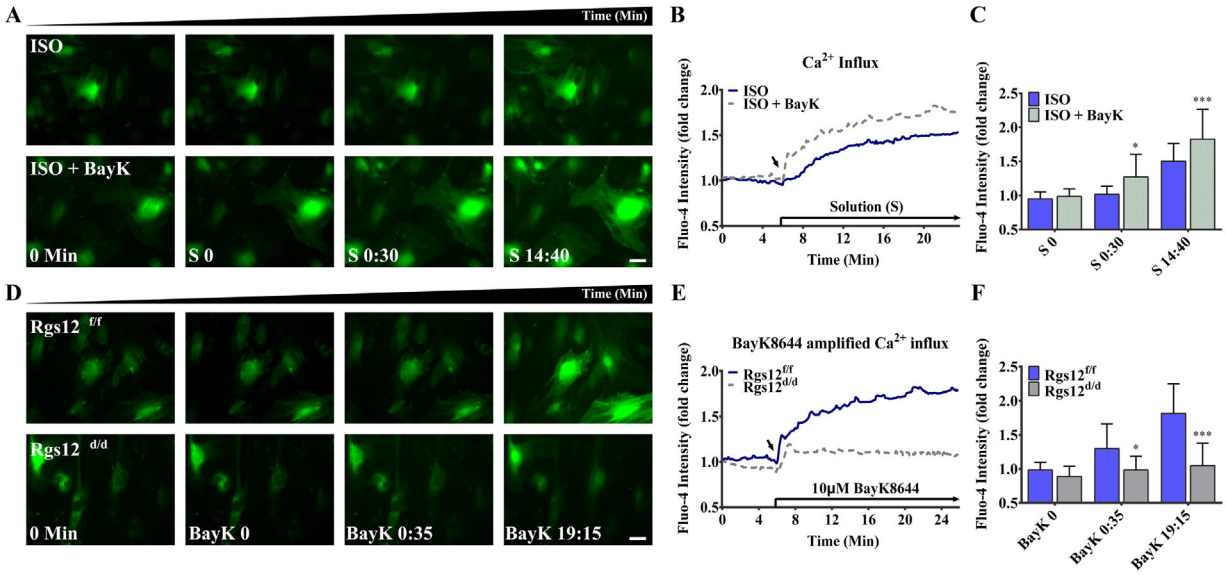

Fig. 6. Deletion of Rgs12 attenuates the Bay K8644-amplified Ca^{2+} influx through L-type Ca^{2+} channel. (*A–C*) Effect of Bay K8644 on intracellular Ca^{2+} in $Rgs12^{f/f}$ OPCs. (*A*) Representative images of intracellular Ca^{2+} in $Rgs12^{f/f}$ OPCs in the presence or absence of 10μM Bay K8644 stimulation. OPCs were incubated in Ca^{2+}-free ISO to reach a stable baseline level of cytosolic Ca^{2+}, and then treated with Bay K8644 in ISO (lower panel) or ISO alone (upper panel). (*B*) Overlay of traces from OPCs. Arrow indicated the time point when different solutions applied (S, started from S 0 min). Data is expressed as a fold change of fluo-4 intensity, accomplished by normalizing each cell's fluorescence intensity to its initial intensity ($n = 28$ cells per group). (*C*) Quantitative analysis of fluo-4 intensity at indicated time point. $^{*}p < 0.05$, $^{***}p < 0.001$ versus cells without Bay K8644. (*D–F*) Effect of Bay K8644 on $Rgs12^{f/f}$ or $Rgs12^{d/d}$ OPCs. (*D*) Representative images of intracellular Ca^{2+} for OPCs before (0 min) and after stimulation of 10μM Bay K8644 (BayK, started from BayK 0 min). OPCs were incubated in Ca^{2+}-free ISO to reach the baseline level of cytosolic Ca^{2+}, and then treated with Bay K8644 in ISO. Upper panel, $Rgs12^{f/f}$ OPCs; lower panel, $Rgs12^{d/d}$ OPCs. (*E*) Overlay of traces from OPCs. Arrow indicates the time point of Bay K8644 application ($n = 28$ cells per group). (*F*) Quantitative analysis of fluo-4 intensity at indicated time point. $^{*}p < 0.05$, $^{***}p < 0.001$ versus $Rgs12^{f/f}$ cells. Scale bars = 50 μm. Quantitative data are presented as mean ± SD.

results suggested ERK severed downstream of Rgs12 and cAMP, and supported our hypothesis that Rgs12 plays an important role during osteogenesis (Fig. 7*K*).

Discussion

Rgs proteins are broadly involved in bone development and remodeling via their influences on OC and OB differentiation and function individually or mutually.[9,20] Our previous study demonstrated that Rgs12 promotes osteoclastogenesis during bone remodeling.[24] Here, to our knowledge, we provide the first evidence to show a close dependency of osteogenesis on the expression of Rgs12, and to reveal the mechanism underlying how Rgs12, through both Ca^{2+} channel-Ca^{2+} oscillation-ERK signaling and traditional Gαi-ERK signaling, promotes OB differentiation and function during osteogenesis. The facilitating role of Rgs12 in bone formation was defined by obvious osteopenia phenotypes in Rgs12 conditional knockout mice ($Osx^{Cre/+}$; $Rgs12^{fl/fl}$) (Fig. 2), and supported by OBs differentiation-deficiency OPCs ($Rgs12^{d/d}$) that underwent in vitro Rgs12 deletion (Fig. 3). Additionally, ectopic expression of Rgs12 in $Rgs12^{d/d}$ demonstrated a restoration of differentiation ability, while enhanced differentiation ability was also observed in normal OPCs ($Rgs12^{f/f}$) with Rgs12 overexpression (Fig. 7*D*, *E*).

We identified Gαi-ERK signaling as one of the pathway that Rgs12 exerted its regulatory role during osteogenesis. Rgs12 is a GTPase-activating protein that enhances the intrinsic GTPase activity of Gαi subunit.[9,20,21] It has been noted that hyperactivation of the Gαi-mediated signaling serves as a negative regulator of OB differentiation through inhibitory action on adenylyl cyclase (AC)-cAMP formation, and eventually leads to a reduction in trabecular bone formation,[23,39] whereas contrarily, Gαs-AC-cAMP signaling is required for OB differentiation.[48,49] In such a way, it would be rational to postulate that the deletion of Rgs12 shrinks GTPase activity toward the Gαi subunit and subsequently eases the inhibitory effect on Gαi-mediated signaling, leading to an osteopenia phenotype. We found that Pi release reduced approximately 53% in $Rgs12^{d/d}$ OPCs compared with control OPCs (Fig. 4*A*), and OS induced-cAMP level was also downregulated (Fig. 4*B*), indicating a dramatic shrink of GTPase activity toward the Gαi subunit and a reduced cAMP formation after Rgs12 deletion. Several studies show that ERK activation serves as downstream effector of Gαi-mediated signaling via membrane recruitment of rap1GAPII and reduction of GTP-bound Rap1.[39,49,50] In OBs, the ERK pathway is a major conduit for conveying information from the extracellular environment to the nucleus, and has been implicated in the response of OBs to a variety of signals, including hormone/growth factor stimulation, extracellular matrix–integrin binding, and mechanical loading.[51–53] ERK activation stimulates OB differentiation and skeletal development through OBs' essential transcription factor, Runx2, which plays an important role during the process.[54,55] Our results are in agreement with these findings. We found a significantly lower expression of p-ERK in $Rgs12^{d/d}$ cells after OS medium stimulation (Fig. 4*F*), and further exhibited inability of OBs differentiation compared to $Osx^{Cre/+}$;

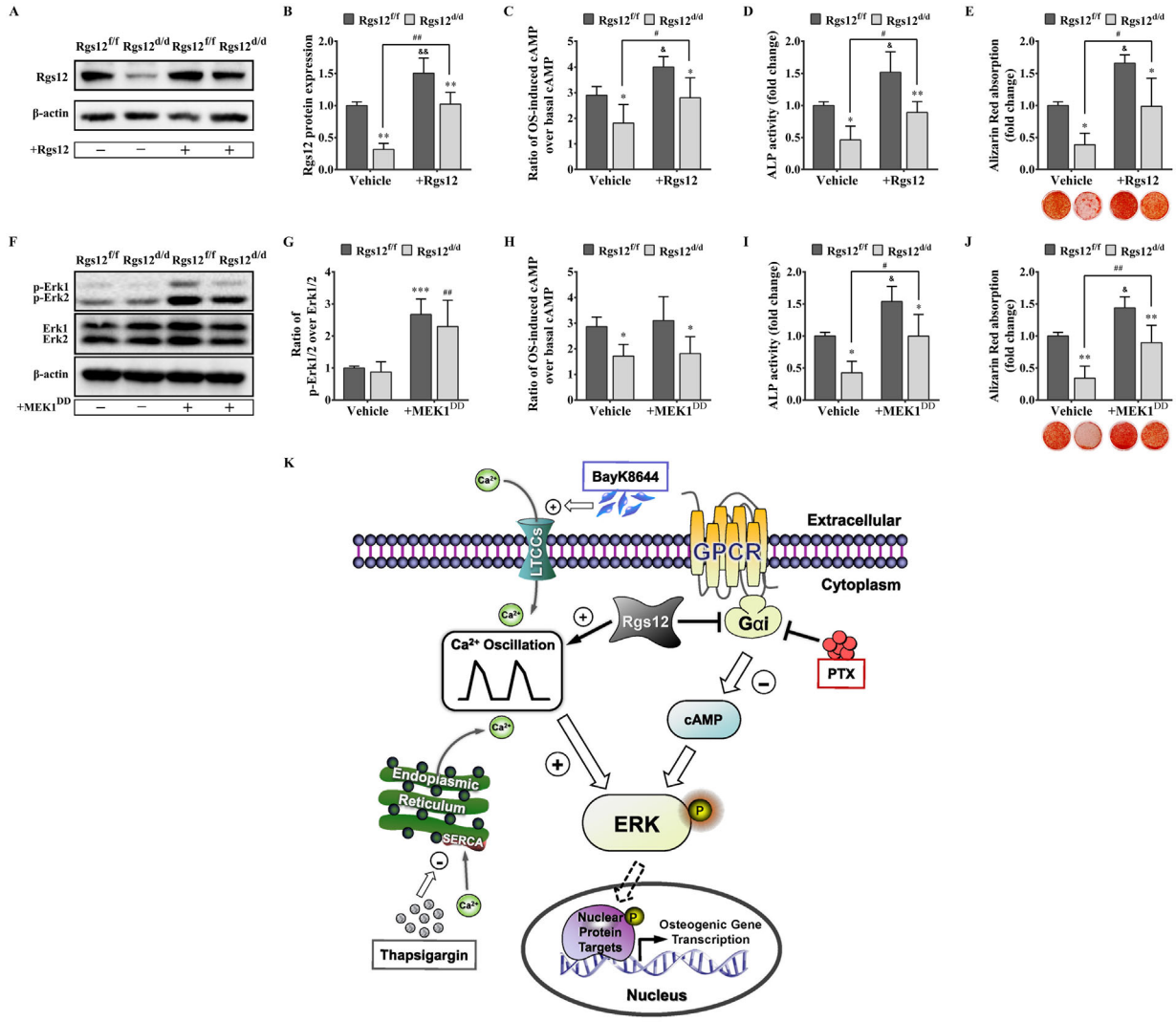

Fig. 7. Ectopic expression of Rgs12 or constitutive ERK activation rescues defective OB differentiation and function. (*A*) WB and quantitative analysis (*B*) showed Rgs12 protein expression in $Rgs12^{f/f}$ and $Rgs12^{d/d}$ OPCs with or without overexpression of Rgs12, normalized to β-actin. (*C*) ELISA showed cAMP of OPCs in response to OS medium stimulation. Cells were starved for 6 hours prior to OS medium stimulation or completed medium stimulation (basal cAMP) for 30 min. (*D*) ALP activity (day 7) and (*E*) Alizarin Red staining and absorption (day 21) of OBs. $^{*}p < 0.05$, $^{**}p < 0.01$ versus $Rgs12^{f/f}$ cells within groups; $^{\&}p < 0.05$, $^{\&\&}p < 0.01$, or $^{\#}p < 0.05$ versus same cells without Rgs12 overexpression; $n = 3$. (*F*) WB and quantitative analysis (*G*) showed p-ERK expression in $Rgs12^{f/f}$ and $Rgs12^{d/d}$ OPCs with or without $MEK1^{DD}$ transfection, normalized to total ERK. $^{***}p < 0.001$ or $\#\#p < 0.01$ versus cells without $MEK1^{DD}$ transfection, $n = 3$. (*H*) ELISA showed cAMP of OPCs in response to OS medium stimulation. (*I*) ALP activity (day 7) and (*J*) Alizarin Red staining and absorption (day 21) of OBs. $^{*}p < 0.05$, $^{**}p < 0.01$ versus $Rgs12^{f/f}$ cells within groups; $^{\&}p < 0.05$ or $\#p < 0.05$, $\#\#p < 0.01$ versus same cells without $MEK1^{DD}$ transfection, $n = 3$. Data are presented as mean ± SD. (*K*) Proposed role of Rgs12-regulated Gαi and Ca^{2+} signaling during OB differentiation.

$Rgs12^{fl/fl}$ cells. PTX treatment of $Rgs12^{d/d}$ cells rescued OB differentiation (Fig. 4*G*), and these rescue effects became even more obvious after ectopic expression of Rgs12 or introducing ERK activation ($MEK1^{DD}$ transfection) in defective OPCs (Fig. 7). cAMP level was also recovered in Rgs12 overexpressed cells but not $MEK1^{DD}$ transfected cells, further confirming ERK acted downstream of Rgs12, and the involvement of the Gαi-mediated ERK signaling pathway in Rgs12 regulated OB differentiation and function.

We also identified Ca^{2+} channel-Ca^{2+} oscillation-ERK signaling as another critical pathway that contributes to the regulatory role of Rgs12 during osteogenesis (Fig. 7*K*). Ca^{2+}, as an intracellular second messenger, impacts nearly every aspect of biological processes through enormous versatility of Ca^{2+} signaling.[16,56] Components of Ca^{2+} signaling, including Ca^{2+} influx through Ca^{2+} channel and Ca^{2+} release from intracellular store, regulate the frequency and amplitude of Ca^{2+} oscillations, which are critical for promoting osteogenesis.[9,12,13,20] Our results showed that Ca^{2+} oscillations were barely detectable in $Rgs12^{d/d}$ OPCs (Fig. 4*C*), indicating an impairment on Ca^{2+} oscillations caused by Rgs12 deletion. We further found that both extracellular Ca^{2+} influx and Ca^{2+} release from the ER store, which contributed as major sources for Ca^{2+} oscillations, were restrained after Rgs12 deletion (Fig. 5). Several studies also demonstrate that these two major Ca^{2+} sources play fundamental roles in regulating OB proliferation, differentiation, and function.[18,20,43,44] Therefore, our work revealed the role of

Rgs12 as a key regulator of Ca^{2+} oscillations during osteogenesis. Moreover, Ca^{2+} enters cytosol through a variety of Ca^{2+} channels; among them, LTCCs have been listed as critical regulators of intracellular Ca^{2+} homeostasis in OBs and are closely associated with the regulation of OB functions.[17,44,45] Our current data corroborated with those finds and further suggested a direct involvement of LTCCs in Rgs12 deletion-caused restraint of Ca^{2+} influx, proved by insufficient performance of LTCCs after Bay K8644 treatment in $Rgs12^{d/d}$ OPCs (Fig. 6*D–F*). ERK also serves as a downstream effector of Ca^{2+} signaling, and the frequencies of Ca^{2+} oscillations were reported to influence Ca^{2+}-mediated activation of Ras and signaling through the ERK/mitogen-activated protein kinase (MAPK) cascade.[19,57] The inactivation of ERK after Rgs12 deletion in OPCs could also be due to the decreased Ca^{2+} signaling originating from LTCCs.

Crosstalk between Gαs, Gαi, and Ca^{2+} signaling has long been reported.[39] Ca^{2+} signaling can exert powerful modulatory actions on cAMP accumulation, especially the termination of cAMP signals, similar to the inhibitory action of the PTX-sensitive Gαi pathway on cAMP accumulation.[40] Intracellular cAMP level could fluctuate during Ca^{2+} oscillation, causing repetitive activation–inactivation cycles that encode information affecting downstream signaling.[40,41] It has been noted that Ca^{2+} sensing receptor (CaR/CaSR) plays a dual role in cAMP signaling, exerting through intracellular Ca^{2+} and PTX-sensitive Gαi pathways.[40] Activation of CaR, in part through the activation of the classic Gαq-PLCβ pathway that leads to increased Ca^{2+} oscillations, promotes OB proliferation.[9,42] Emerging evidence shows that Gαi3 mutants with defective GTP binding and lower GTPase activity can block the Gαq-PLC-Ca^{2+} signaling pathway by forming an unproductive complex.[50,58] In our work, we also found lower GTPase activity toward Gαi after Rgs12 deletion. Yamamura and colleagues[59] reported that Bay K8644 can directly activate CaR, increasing CaR-mediated cytosolic Ca^{2+} concentration. Studies also describe reciprocal relationship between CaR and LTCC due to increased spatial interaction, or change of extracellular calcium.[60–63] Our results agreed with these finds because Bay K8644 directly increased cytosolic Ca^{2+} in $Rgs12^{f/f}$ OPCs; however, whether CaR involved in cytosolic Ca^{2+} restraint after Rgs12 deletion is uncharted in the current study, as well as the deletion effect on LTCC subunits, and more studies are needed.

An interesting phenomenon from our present and previous studies is that Rgs12 deletion impaired Ca^{2+} oscillations in both OBs and OCs, leading to either osteopenia or osteopetrosis phenotype.[24] One limitation of the osteopenia phenotype in current study is the use of Osx-Cre transgenic mice to delete Rgs12 in OB lineage. Although several studies have proved that skeletal defects originated from Osx-Cre transgenic mice recovered after 12 weeks old,[28–31] it is worth noting that the effects of Osx-Cre on early skeletal development, and at some extent on cell types other than OBs may leave phenotypic differences in adult mice.[64,65] More specific OB lineage Cre transgenic mice need to be developed. Taken together, our results reveal a crucial role of Rgs12 in OB differentiation and bone formation via Ca^{2+} channel/oscillation and Gαi-ERK signaling, and highlight Rgs12 as a potential therapeutic target for skeletal abnormalities.

Disclosures

ZL, TL, AG, NG, CF, JL, Shuting Y, CM, YPL, MO and SY have no conflicts of interest to disclose.

Acknowledgments

This work was supported by grants from the NIH (National Institute on Aging [NIA], AG048388 to SY; National Institute of Arthritis and Musculoskeletal and Skin Diseases [NIAMS], AR066101 to SY; National Institute of Dental and Craniofacial Research [NIDCR], DE023105 to SY).

Authors' roles: Study design: SY, MO, CM, and YPL. Study conduct: ZL, TL, AG, NG, CF, JL, and STY. Data collection: ZL, TL, AG, and CF. Data analysis: ZL, TL, and NG. Data interpretation: ZL, TL, AG, NG, and CF. Drafting manuscript: ZL and AG. Revising manuscript content: SY, MO, and CM. Approving final version of manuscript: SY, MO, YPL, and CM. ZL, TL, AG, and SY take responsibility for the integrity of the data analysis.

References

1. Zaidi M. Skeletal remodeling in health and disease. Nat Med. 2007;13(7):791–801.
2. Rachner TD, Khosla S, Hofbauer LC. Osteoporosis: now and the future. Lancet. 2011;377(9773):1276–87.
3. Seeman E. Pathogenesis of bone fragility in women and men. Lancet. 2002;359(9320):1841–50.
4. Khosla S, Riggs BL. Pathophysiology of age-related bone loss and osteoporosis. Endocrinol Metab Clin North Am. 2005;34(4):1015–30, xi.
5. Marie PJ. Osteoblast dysfunctions in bone diseases: from cellular and molecular mechanisms to therapeutic strategies. Cell Mol Life Sci. 2015;72(7):1347–61.
6. Riggs BL, Parfitt AM. Drugs used to treat osteoporosis: the critical need for a uniform nomenclature based on their action on bone remodeling. J Bone Miner Res. 2005;20(2):177–84.
7. Kawai M, Modder UI, Khosla S, Rosen CJ. Emerging therapeutic opportunities for skeletal restoration. Nat Rev Drug Discov. 2011;10(2):141–56.
8. Green JT, Mills AM. Osteogenic tumors of bone. Semin Diagn Pathol. 2014;31(1):21–9.
9. Jules J, Yang S, Chen W, Li YP. Role of regulators of G protein signaling proteins in bone physiology and pathophysiology. Prog Mol Biol Transl Sci. 2015;133:47–75.
10. Raucci A, Bellosta P, Grassi R, Basilico C, Mansukhani A. Osteoblast proliferation or differentiation is regulated by relative strengths of opposing signaling pathways. J Cell Physiol. 2008;215(2):442–51.
11. Hanna H, Andre FM, Mir LM. Electrical control of calcium oscillations in mesenchymal stem cells using microsecond pulsed electric fields. Stem Cell Res Ther. 2017;8(1):91.
12. Suzuki T, Notomi T, Miyajima D, et al. Osteoblastic differentiation enhances expression of TRPV4 that is required for calcium oscillation induced by mechanical force. Bone. 2013;54(1):172–8.
13. Sun S, Liu Y, Lipsky S, Cho M. Physical manipulation of calcium oscillations facilitates osteodifferentiation of human mesenchymal stem cells. FASEB J. 2007;21(7):1472–80.
14. Wang X, Huang G, Luo X, Penninger JM, Muallem S. Role of regulator of G protein signaling 2 (RGS2) in Ca(2+) oscillations and adaptation of Ca(2+) signaling to reduce excitability of RGS2-/- cells. J Biol Chem. 2004;279(40):41642–9.
15. Catterall WA. Voltage-gated calcium channels. Cold Spring Harb Perspect Biol. 2011;3(8):a003947.
16. Prakriya M, Lewis RS. Store-operated calcium channels. Physiol Rev. 2015;95(4):1383–436.
17. Sun Z, Cao X, Zhang Z, et al. Simulated microgravity inhibits L-type calcium channel currents partially by the up-regulation of miR-103 in MC3T3-E1 osteoblasts. Sci Rep. 2015;5:8077.
18. Zayzafoon M. Calcium/calmodulin signaling controls osteoblast growth and differentiation. J Cell Biochem. 2006;97(1):56–70.

19. Mulvaney JM, Zhang T, Fewtrell C, Roberson MS. Calcium influx through L-type channels is required for selective activation of extracellular signal-regulated kinase by gonadotropin-releasing hormone. J Biol Chem. 1999;274(42):29796–804.
20. Keinan D, Yang S, Cohen RE, Yuan X, Liu T, Li YP. Role of regulator of G protein signaling proteins in bone. Front Biosci (Landmark Ed). 2014;19:634–48.
21. Snow BE, Hall RA, Krumins AM, et al. GTPase activating specificity of RGS12 and binding specificity of an alternatively spliced PDZ (PSD-95/Dlg/ZO-1) domain. J Biol Chem. 1998;273(28):17749–55.
22. Kimple RJ, De Vries L, Tronchere H, et al. RGS12 and RGS14 GoLoco motifs are G alpha(i) interaction sites with guanine nucleotide dissociation inhibitor Activity. J Biol Chem. 2001;276(31):29275–81.
23. Peng J, Bencsik M, Louie A, et al. Conditional expression of a Gi-coupled receptor in osteoblasts results in trabecular osteopenia. Endocrinology. 2008;149(3):1329–37.
24. Yuan X, Cao J, Liu T, et al. Regulators of G protein signaling 12 promotes osteoclastogenesis in bone remodeling and pathological bone loss. Cell Death Differ. 2015;22(12):2046–57.
25. Yang S, Li YP, Liu T, et al. Mx1-cre mediated Rgs12 conditional knockout mice exhibit increased bone mass phenotype. Genesis. 2013;51(3):201–9.
26. Yang S, Li YP. RGS12 is essential for RANKL-evoked signaling for terminal differentiation of osteoclasts in vitro. J Bone Miner Res. 2007;22(1):45–54.
27. Yuan X, Cao J, He X, et al. Ciliary IFT80 balances canonical versus non-canonical hedgehog signalling for osteoblast differentiation. Nat Commun. 2016;7:11024.
28. Sinha KM, Zhou X. Genetic and molecular control of osterix in skeletal formation. J Cell Biochem. 2013;114(5):975–84.
29. Davey RA, Clarke MV, Sastra S, et al. Decreased body weight in young Osterix-Cre transgenic mice results in delayed cortical bone expansion and accrual. Transgenic Res. 2012;21(4):885–93.
30. Wang L, Mishina Y, Liu F. Osterix-Cre transgene causes craniofacial bone development defect. Calcif Tissue Int. 2015;96(2):129–37.
31. Liu F, Fang F, Yuan H, et al. Suppression of autophagy by FIP200 deletion leads to osteopenia in mice through the inhibition of osteoblast terminal differentiation. J Bone Miner Res. 2013;28(11):2414–30.
32. Khoshniat S, Bourgine A, Julien M, et al. Phosphate-dependent stimulation of MGP and OPN expression in osteoblasts via the ERK1/2 pathway is modulated by calcium. Bone. 2011;48(4):894–902.
33. Li Z, Li C, Zhou Y, et al. Advanced glycation end products biphasically modulate bone resorption in osteoclast-like cells. Am J Physiol Endocrinol Metab. 2016;310(5):E355–66.
34. de Bakker CM, Altman-Singles AR, Li Y, Tseng WJ, Li C, Liu XS. Adaptations in the microarchitecture and load distribution of maternal cortical and trabecular bone in response to multiple reproductive cycles in rats. J Bone Miner Res. 2017;32(5):1014–26.
35. Chandra A, Lin T, Young T, et al. Suppression of sclerostin alleviates radiation-induced bone loss by protecting bone-forming cells and their progenitors through distinct mechanisms. J Bone Miner Res. 2017;32(2):360–72.
36. Ping S, Liu S, Zhou Y, et al. Protein disulfide isomerase-mediated apoptosis and proliferation of vascular smooth muscle cells induced by mechanical stress and advanced glycosylation end products result in diabetic mouse vein graft atherosclerosis. Cell Death Dis. 2017;8(5):e2818.
37. Gomez NM, Lu W, Lim JC, et al. Robust lysosomal calcium signaling through channel TRPML1 is impaired by lysosomal lipid accumulation. FASEB J. 2018;32(2):782–94.
38. Lin SJ, Chiang MC, Shih HY, et al. Regulator of G protein signaling 2 (Rgs2) regulates neural crest development through Ppardelta-Sox10 cascade. Biochim Biophys Acta. 2017;1864(3):463–74.
39. Hsiao EC, Millard SM, Nissenson RA. Gs/Gi regulation of bone cell differentiation: review and insights from engineered receptors. Horm Metab Res. 2016;48(11):689–99.
40. Gerbino A, Ruder WC, Curci S, Pozzan T, Zaccolo M, Hofer AM. Termination of cAMP signals by Ca2+ and G(alpha)i via extracellular Ca2+ sensors: a link to intracellular Ca2+ oscillations. J Cell Biol. 2005;171(2):303–12.
41. Cooper DM, Mons N, Karpen JW. Adenylyl cyclases and the interaction between calcium and cAMP signalling. Nature. 1995;374(6521):421–4.
42. Caverzasio J, Palmer G, Suzuki A, Bonjour JP. Evidence for the involvement of two pathways in activation of extracellular signal-regulated kinase (Erk) and cell proliferation by Gi and Gq protein-coupled receptors in osteoblast-like cells. J Bone Miner Res. 2000;15(9):1697–706.
43. Dolmetsch RE, Lewis RS. Signaling between intracellular Ca2+ stores and depletion-activated Ca2+ channels generates [Ca2+]i oscillations in T lymphocytes. J Gen Physiol. 1994;103(3):365–88.
44. Freisinger CM, Schneider I, Westfall TA, Slusarski DC. Calcium dynamics integrated into signalling pathways that influence vertebrate axial patterning. Philos Trans R Soc Lond B Biol Sci. 2008;363(1495):1377–85.
45. Park R, Ji JD. Calcium channels: the potential therapeutic targets for inflammatory bone destruction of rheumatoid arthritis. Inflamm Res. 2016;65(5):347–54.
46. Boehm JS, Zhao JJ, Yao J, et al. Integrative genomic approaches identify IKBKE as a breast cancer oncogene. Cell. 2007;129(6):1065–79.
47. Al-Ayoubi AM, Zheng H, Liu Y, Bai T, Eblen ST. Mitogen-activated protein kinase phosphorylation of splicing factor 45 (SPF45) regulates SPF45 alternative splicing site utilization, proliferation, and cell adhesion. Mol Cell Biol. 2012;32(14):2880–93.
48. Sakamoto A, Chen M, Nakamura T, Xie T, Karsenty G, Weinstein LS. Deficiency of the G-protein alpha-subunit G(s)alpha in osteoblasts leads to differential effects on trabecular and cortical bone. J Biol Chem. 2005;280(22):21369–75.
49. Luttrell LM. Reviews in molecular biology and biotechnology: transmembrane signaling by G protein-coupled receptors. Mol Biotechnol. 2008;39(3):239–64.
50. Blaukat A, Barac A, Cross MJ, Offermanns S, Dikic I. G protein-coupled receptor-mediated mitogen-activated protein kinase activation through cooperation of Galpha(q) and Galpha(i) signals. Mol Cell Biol. 2000;20(18):6837–48.
51. Hurley MM, Marcello K, Abreu C, Kessler M. Signal transduction by basic fibroblast growth factor in rat osteoblastic Py1a cells. J Bone Miner Res. 1996;11(9):1256–63.
52. Takeuchi Y, Suzawa M, Kikuchi T, Nishida E, Fujita T, Matsumoto T. Differentiation and transforming growth factor-beta receptor down-regulation by collagen-alpha2beta1 integrin interaction is mediated by focal adhesion kinase and its downstream signals in murine osteoblastic cells. J Biol Chem. 1997;272(46):29309–16.
53. You J, Reilly GC, Zhen X, et al. Osteopontin gene regulation by oscillatory fluid flow via intracellular calcium mobilization and activation of mitogen-activated protein kinase in MC3T3-E1 osteoblasts. J Biol Chem. 2001;276(16):13365–71.
54. Ge C, Xiao G, Jiang D, Franceschi RT. Critical role of the extracellular signal-regulated kinase-MAPK pathway in osteoblast differentiation and skeletal development. J Cell Biol. 2007;176(5):709–18.
55. Xiao G, Jiang D, Gopalakrishnan R, Franceschi RT. Fibroblast growth factor 2 induction of the osteocalcin gene requires MAPK activity and phosphorylation of the osteoblast transcription factor, Cbfa1/Runx2. J Biol Chem. 2002;277(39):36181–7.
56. Berridge MJ, Lipp P, Bootman MD. The versatility and universality of calcium signalling. Nat Rev Mol Cell Biol. 2000;1(1):11–21.
57. Kupzig S, Walker SA, Cullen PJ. The frequencies of calcium oscillations are optimized for efficient calcium-mediated activation of Ras and the ERK/MAPK cascade. Proc Natl Acad Sci U S A. 2005;102(21):7577–82.
58. Marivin A, Leyme A, Parag-Sharma K, et al. Dominant-negative Galpha subunits are a mechanism of dysregulated heterotrimeric G protein signaling in human disease. Sci Signal. 2016;9(423):ra37.
59. Yamamura A, Yamamura H, Guo Q, et al. Dihydropyridine Ca(2+) channel blockers increase cytosolic [Ca(2+)] by activating Ca(2+)-sensing receptors in pulmonary arterial smooth muscle cells. Circ Res. 2013;112(4):640–50.
60. Parkash J, Asotra K. L-histidine sensing by calcium sensing receptor inhibits voltage-dependent calcium channel activity and insulin secretion in beta-cells. Life Sci. 2011;88(9-10):440–6.

61. Freichel M, Zink-Lorenz A, Holloschi A, Hafner M, Flockerzi V, Raue F. Expression of a calcium-sensing receptor in a human medullary thyroid carcinoma cell line and its contribution to calcitonin secretion. Endocrinology. 1996;137(9):3842–8.

62. Jorgensen NR, Teilmann SC, Henriksen Z, Civitelli R, Sorensen OH, Steinberg TH. Activation of L-type calcium channels is required for gap junction-mediated intercellular calcium signaling in osteoblastic cells. J Biol Chem. 2003;278(6):4082–6.

63. Koori K, Maeda H, Fujii S, et al. The roles of calcium-sensing receptor and calcium channel in osteogenic differentiation of undifferentiated periodontal ligament cells. Cell Tissue Res. 2014;357(3):707–18.

64. Chen J, Shi Y, Regan J, Karuppaiah K, Ornitz DM, Long F. Osx-Cre targets multiple cell types besides osteoblast lineage in postnatal mice. PLoS ONE. 2014;9(1):e85161.

65. Huang W, Olsen BR. Skeletal defects in Osterix-Cre transgenic mice. Transgenic Res. 2015;24(1):167–72.